AUTOMATION OF THE PATCH-CLAMP TECHNIQUE: TECHNICAL VALIDATION THROUGH CHARACTERIZATION OF VOLTAGE-GATED POTASSIUM CHANNELS AND LIGAND-GATED ION CHANNELS

sophion

SOPHION BIOSCIENCE A/S
Baltorpvej 154
DK-2750 Ballerup
DENMARK
info@sophion.dk
www.sophion.dk

KAREN KRZYWKOWSKI | RIKKE L. SCHRØDER | TRINE LJUNGSTRØM | JONATAN KUTCHINSKY | SØREN FRIIS | MARGIT ASMILD | RAFAEL TABORYSKI | SIMON PEDERSEN | RAS K. VESTERGAARD | RASMUS B. JACOBSEN | NATHALIE HÉLIX | CLAUS B. SØRENSEN | MORTEN BECH | JEPPE K. CHRISTENSEN | SIMON DUBEAU | NIELS J. WILLUMSEN

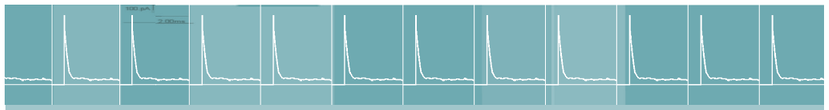

The QPatch™ is a powerful ion channel screening system, which was developed through extensive automation of the conventional patch clamp technique. Whole-cell current measurements take place on a disposable 16-channel QPlate™ in MTP format. Later, also a 48-channel QPlate will be available. Automation has been achieved by (i) employing planar silicon chips rather than traditional glass micropipettes, by (ii) elimination and/or simplification of a number of time-consuming tasks, e.g. visual cell selection and pipette tip localisation, manual microscope-aided pipette positioning and cell contact establishment, and subsequent gigaseal and whole-cell formation, and by (iii) cell preparation directly on the QPatch platform. We here report whole-cell current data from cultured cell lines expressing a number of voltage- or ligand-gated ion channels. The data were obtained on either complete 16-channel QPlates or on single chip assemblies (1-channel prototype).

MATERIALS

ION CHANNEL PROTEINS

For patch clamp measurements were used a number of different ion channels: Voltage gated ion channels (VGIC): hERG, KCNQ4. Ligand gated ion channels (LGIC): $GABA_A$-R, nACh-R, ASIC

CELL CULTURES

The ion channels were expressed in either HEK-293 or CHO-k1 cells. These cell lines were grown according to standard culturing protocols (Kutchinsky et al., Assay and Drug Development Technologies 1:685-693, 2003). All cells were grown at 37°C. After harvest, cells could be kept for up to 4 hours in the cell storage facility on the QPatch platform with no change in quality or ability to form gigaseals.

ELECTROPHYSIOLOGY

Whole-cell measurements were done either on single planar silicon chips or on complete 16-channel QPlates (Figure 1D; Kutchinsky et al., 2003) with either a 16-channel Sophion patch clamp amplifier or with a HEKA (EPC-9, HEKA Elektronik, Germany) commercial amplifier. The chips had micro-etched patch clamp holes with diameters of approximately 1 µm (Figure 1A) and resistances of 2.04±0.02 MΩ (N=274) in symmetrical physiological saline.

SOLUTIONS AND DRUGS

The physiological Ringer solutions consisted of (in mM). Extracellular Na^+ Ringer: 140 NaCl, 4 KCl, 2 $CaCl_2$, 1 $MgCl_2$, 10 HEPES (pH 7.4). Intracellular K^+ Ringer: 120 KCl, 5.4 $CaCl_2$, 1.8 $MgCl_2$ 30/10 KOH/EGTA, 10 HEPES, 4 ATP, 0.4 GTP (pH 7.2). Verapamil was from Sigma, Switzerland. rBeKm-1 was from Alomone Labs, Israel. GABA and retigabine were from NeuroSearch, Denmark. In LGIC experiments solutions were added in 2 µL volumes by an autosampler.

FIG. 1. THE QPatch PATCH-CLAMP SCREENING SYSTEM

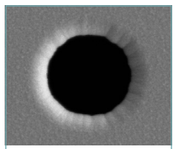

A. Microetched patch-clamp hole in a surface-coated silicon chip. Diameter ~1µm.

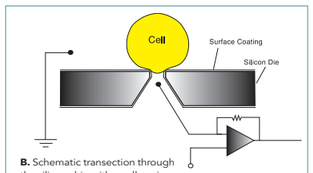

B. Schematic transection through the silicon chip with a cell positioned at the patch-clamp hole.

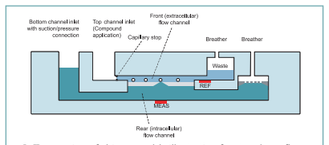

C. Transection of chip assembly illustrating front and rear flow channels, capillary stop, and reference and measuring electrode (REF and MEAS). Both electrodes connect to bottom site for interfacing to QPatch amplifier.

D. The disposable 16-channel QPlate.

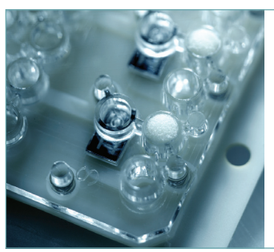

E. Detail of QPlate showing top view of two measurement sites (assemblies).

F. The complete QPatch™ screening station.

FIG. 2. GIGASEAL AND WHOLE-CELL CONFIGURATION WITH QPatch

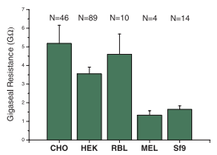

A. The QPatch technology has been successfully used for patch-clamp recordings from a number of different cell lines.

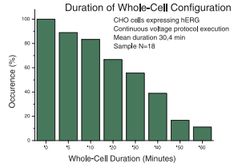

B. Once established the whole-cell is stable. The mean gigaseal lifetime for this sample was 30.4 minutes. Lifetimes in excess of two hours have been observed. CHO cells expressing hERG potassium channels were used.

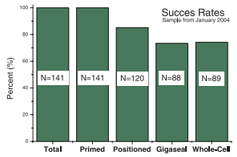

C. Success rates for (i) priming flow channels, (ii) positioning of a cell, (iii) gigaseal formation, and (iv) whole-cell formation. HEK cells expressing KCNQ4 K^+ channels were used. In some cases the whole-cell was established directly with no preceding gigaseal phase – explaining that the whole-cell success rate exceeds the gigaseal success rate.

FIG. 3. SCREENING WITH QPatch: MEASUREMENTS OF KCNQ4 CURRENTS ON A 16-CHANNEL QPlate

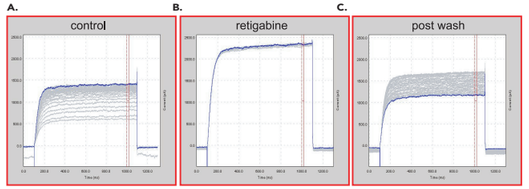

A,B,C. KCNQ4 current sweeps recorded in the pre- and absence of the KCNQ4 activator retigabine (10 µM). The compound application volume was 5 µL followed by 10 µL Na^+ Ringer (wash). The current was activated at -30 mV (1s) from a holding potential of -90 mV. Deactivation at -120 mV (200 ms). Blue current sweeps are representative for each application period.

D. The resistance (R) is measured continuously after priming. R_{Omp} is initially 1.3 MΩ. At t=82 s a cell is positioned by suction (see Panel E), and R increases to >1GΩ. During the following 30 s the gigaseal is improved (increased and stabilized). R is monitored every second.

E. Cell positioning and gigaseal- and whole-cell formation are accomplished by application of negative hydrostatic pressure (blue graph) to the rear flow channel. Until cell positioning, a small positive pressure (8 mbar) is applied to keep the chip hole uncontaminated. For cell positioning a brief negative pressure pulse (-70 mbar) is applied at t=82 s. In the example shown, the gigaseal was formed spontaneously without the need for additional pressure modulations. Two pulses of -150 and -170 mbar, respectively, were subsequently applied to obtain whole-cell configuration. Chip and cell capacitances (red graph) were cancelled subsequent to gigaseal and whole-cell formation.

F. Summary of the effect of retigabine. Whole-cell currents were recorded at the cursors in A,B and C.

FIG. 4. PATCH-CLAMPING WITH QPatch: CONCENTRATION-RESPONSE RELATIONSHIPS FOR hERG CHANNEL BLOCKERS

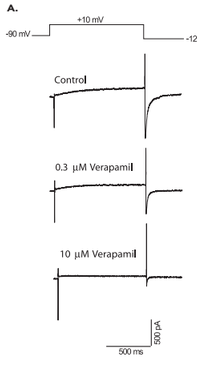

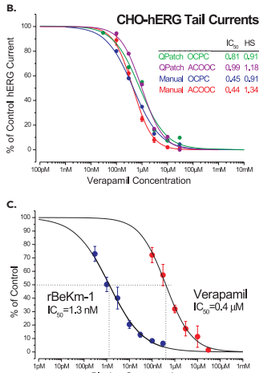

A. Original whole-cell current recordings from a CHO cell expressing hERG potassium channels. A single-channel QPatch prototype was used together with Sophion's QPatch amplifier for these recordings. The currents were recorded in response to the voltage protocol shown on top. In the two lower panels the hERG currents were recorded in the presence of the blocker 0.3 and 10 µM verapamil.

B. Comparison of concentration-response relationships obtained with QPatch and with conventional patch-clamp. Two protocols were employed: either one concentration per cell (OCPC) or all concentrations on one cell (ACOOC, sequential application). IC_{50} is given in µM. HS: Hill Slope.

C. Concentration-response relationships for verapamil and the potent hERG blocker rBeKm-1 (a scorpion venom) measured with the QPatch screening system.

FIG. 5. CAN QPatch MEASURE LIGAND-GATED ION CHANNEL CURRENTS? COMPUTER MODEL PREDICTIONS

Fluid application in the QPatch screening system is accomplished through flow channels in the QPlate assembly (Figures 1C and 5A). For measurement of current transients from ligand-gated ion channels, fast ligand application is required. In conventional patch-clamp this is often achieved by usage of a piezo stepper. This option is not possible in a fixed flow channel based system.

A computer model was developed to evaluate whether proper LGIC current responses can be expected when using the QPatch technology. We examined the effects of the following parameters on the recorded LGIC current:

1. the ligand concentration profile
2. the time it takes for the ligand to reach the cell (dependent on flow rate and travel distance)
3. the characteristics of the LGIC (open-state probability and desensitisation time constants)

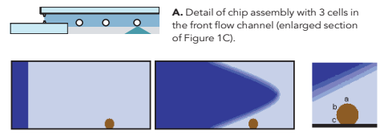

A. Detail of chip assembly with 3 cells in the front flow channel (enlarged section of Figure 1C).

B. Computer simulation of the ligand concentration profile in the front channel at t=0 **(left panel)** and just before the ligand reach the cell **(middle panel)**. The ellipsoid shape with fuzzy edges is created by a laminar flow friction and by diffusion. Letters a,b and c denote upper, middle, and lower position on the cell surface **(right panel)**.

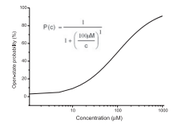

C. Open-state probability for the LGIC as function of ligand concentration. This dose-response type relationship was used for the LGIC current to simulate application of 1µM ligand to the cell.

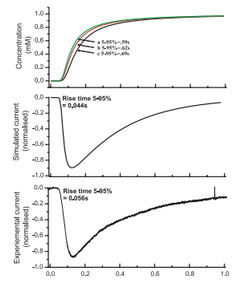

D. Upper panel: Change in local ligand concentration at positions a,b and c (see Figure 5B) following application of 1 µM of the ligand in the compound delivery well of the QPlate. **Middle panel:** Simulation of the LGIC current in response to 1 µM ligand to the QPlate. The desensitisation time constant was set to 330 ms. **Lower panel:** Experimental current recorded from a HEK293-cell expressing nicotinic acetylcholine receptor (nAChR) $\alpha\alpha\beta\varepsilon\delta$. The response was induced by 1 µM acetylcholine.

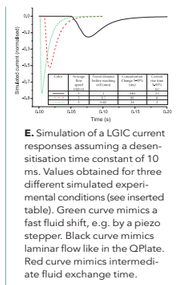

E. Simulation of a LGIC current responses assuming a desensitisation time constant of 10 ms. Values obtained for three different simulated experimental conditions (see inserted table). Green curve mimics a fast fluid shift, e.g. by a piezo stepper. Black curve mimics laminar flow like in the QPlate. Red curve mimics intermediate fluid exchange time.

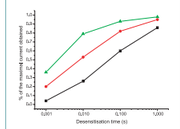

F. Maximal LGIC currents as function of the desensitisation time constant. Coloured graphs refer to conditions described in Figure 5E.

The simulations predict that

- The desensitisation time constant affects the maximal LGIC current measured
- A setup with fast concentration shift will be less sensitive to the effect of desensitisation time
- Even with relatively slow concentration shifts, fast LGIC rise times can be measured

FIG. 6. RECORDING OF LIGAND-GATED ION CHANNEL CURRENTS

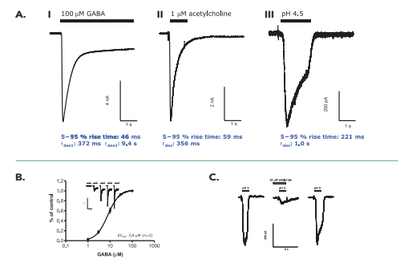

A. Representative current responses induced by: I: 100 µM GABA in HEK293 cells expressing the $\alpha_1\beta_2\gamma_2$ $GABA_A$ receptor; II: 1 µM acetylcholine in HEK293 cells expressing the $\alpha_3\beta_4$ nACh receptor; III: the lowering of pH to 4.5 from a holding of 7.4 in HEK293 cells endogenously expressing the ASIC1a receptor. The cells were voltage clamped at -60 mV in the whole-cell configuration.

B. Concentration response relationship for GABA at HEK293 cells expressing $\alpha_1\beta_2\gamma_2$ $GABA_A$ receptors. Values were normalized to maximum currents (100 µM GABA; 100 %) and represent the mean ± SEM of 3 separate experiments. Left panel shows the current responses induced by 1 – 100 µM GABA. Agonist exposure is indicated by horizontal bars.

C. Amiloride inhibition of current responses induced by lowering pH from 7.4 to 5 in HEK293 endogenously expressing ASIC1a receptors. After attainment of responses of repeatable amplitude (only one response shown), 10 µM amiloride was included in the solution as indicated by the white horizontal bar. The cells were voltage clamped at -60 mV in the whole-cell configuration.

D. Complete recovery obtained for $GABA_A$ receptor-mediated currents recorded at QPlates. Representative current responses induced by 10 µM GABA in HEK293 cells expressing the $\alpha_1\beta_2\gamma_2$ $GABA_A$ receptor. The cells were voltage clamped at -60 mV in the whole-cell configuration and current responses were induced by applying 2 µL external ringer containing 10 µM GABA to the QPlate. The GABA containing solution was efficiently removed from the QPlate by four applications of 2 µL washing ringer and complete recovery obtained for a second current response induced by 10 µM GABA. At the right is shown how liquids are organized in the application pipette.

SUMMARY

High-quality whole-cell recordings from a number of ion channels expressed in cultured cell lines have demonstrated that voltage-gated as well as ligand-gated ion channel proteins can be efficiently targeted by the QPatch screening technology. Automation of the patch-clamp technique will substantially increase throughput in future ion channel drug discovery